Article

pH-Driven Polymorphic Behaviour of the Third PDZ Domain of PSD95: The Role of Electrostatic Interactions

Mª Carmen Salinas-García [1], Marina Plaza-Garrido [1], Jose A. Gavira [2], Javier Murciano-Calles [3], Montserrat Andújar-Sánchez [1], Emilia Ortiz-Salmerón [1], Jose C. Martinez [3] and Ana Cámara-Artigas [1,*]

1   Department of Chemistry and Physics, Agrifood Campus of International Excellence (ceiA3) and CIAMBITAL, University of Almeria, Carretera de Sacramento s/n, 04120 Almeria, Spain
2   Laboratory for Crystallography Studies, IACT, CSIC-UGR, Avda. de las Palmeras, 4, Armilla, 18100 Granada, Spain
3   Department of Physical Chemistry, University of Granada, Fuentenueva s/n, 18071 Granada, Spain
*   Correspondence: acamara@ual.es

Abstract: The PDZ domains are modular domains that recognise short linear C-terminal sequences in proteins that organise the formation of complex multi-component assemblies. We have crystallised the third PDZ domain of the neuronal postsynaptic density-95 protein (PSD95-PDZ3) at mildly acidic pH conditions and obtained up to four polymorphs. Thus, below pH 4.0, the protein crystallised into prism-shaped crystals that belonged to the trigonal space group $P3_112$. In contrast, above this pH value, the crystals' shape changes to long needles belonging to the monoclinic $P2_1$ and two different orthorhombic packings of the $P2_12_12_1$ space group. In addition, all the polymorphs share the main crystallographic interface, where the sidechain of the Asp332 imitates the binding of the C-terminal moiety to the canonical binding motif. Furthermore, we have analysed how changes in the ionisation state of some specific residues might be critical for crystallising the different polymorphs. The analysis of these polymorphs provides clues on the relevance of specific protein-protein interactions in protein crystallisation. However, these structures allow dissecting those electrostatic interactions that play a role in the conformation adopted by some residues and the extra-domain components upon binding C-terminal sequences.

Keywords: PDZ domain; X-ray structures; conformational changes; polymorphs; electrostatic interactions

1. Introduction

The modular domains play a critical role in many cellular processes by establishing protein-protein interactions (PPIs) in the cell. However, high-throughput screening (HTS) methods have produced considerable information to determine how these interactions occur, and knowing their molecular basis is critical for developing new drugs [1]. Moreover, studying these interactions is also essential for improving crystal quality, as growing high-quality crystals is hampered by the small number and weak nature of the interactions that hold together the protein molecules. Furthermore, because modular domains are implied in the recognition of specific sequences, it is expected that the residues involved in these inter-protein interactions are also prone to participate in crystal contacts. Some examples of crystal structures of small modular domains in which crystal contacts show pseudo-binding interactions have been described, such as the SH3 domain [2,3] and the PDZ domain [4]. Specifically, protein-protein interactions have been exploited as an advantage in crystallising the PDZ domains [5].

The PDZ domains comprise a significant group of small modular domains participating in cell PPIs regulating various cellular processes [6]. These domains recognise the C-terminal residues of their target proteins with a low affinity ranging from 1 to 100 μM. The PDZ domain is present in numerous proteins as the scaffolding of receptors and signalling proteins. Its canonical fold contains approximately 80–100 amino acids with the structure of

a partially open barrel fold composed of six β-strands and two α-helices. The PDZ binding motifs (PBM) are usually described by a consensus sequence of four residues that bind as an antiparallel β-strand in an elongated groove between the α2 helix and the β2 strand. The C-terminal carboxylate of the PBM interacts with a highly conserved GLGF motif found within the β1-β2 connecting loop [7]. This motif is recognised as the canonical binding site for PDZ domains. Interestingly, although PDZ domains typically recognise C-terminal carboxyl motifs, some also recognise internal sequence motifs of target proteins [8–11].

In addition, from a biophysical and structural point of view, one of the best-characterised PDZ domains is the third PDZ domain of the postsynaptic density protein 95 (PSD95-PDZ3). The PSD95 belongs to the membrane-associated guanylate kinase (MAGUK) family and is composed of one guanylate kinase domain (GK), three PDZ domains, and one SH3 domain [12]. The third PDZ domain of this protein shows an extra carboxyl-terminal α-helix, α3, packed against the PDZ fold, which acts as a linker between the PDZ domain and the SH3 domain. However, this helix seems to be a regulatory element in the folding and binding of this domain since its removal favours oligomerization of a folding intermediate detected in PSD95-PDZ3 and decreases binding affinity [13–16]. This α3 helix has been proposed to be implied in an allosteric network where specific electrostatic interactions might play a crucial role [17]. Previous structural studies on the PSD95-PDZ3 show significant differences in the α3 helix modelling [4,7,18]. These crystal structures reveal that these changes are also associated with the sequence of the β-turn connecting strands β2-β3 (Glu331-Glu334) [4]. In addition, some structures have a modified aspartate residue in position 332, that is modelled as a succinimide [18]. In order to study the effect of this modification, we solved the structures of the unmodified protein and two mutants at this position, Asp332Pro and Asp332Gly. Consequently, in those structures where Asp332 was present, its sidechain emulated the binding of the terminal carboxylate in the PBMs [4]. As Asp332 is located at the tip of the second β-turn, flanked by two glutamate residues, it is expected that the ionisation state of these residues will be affected not only by the pH but also by the ionisation state of the neighbouring residues.

In this work, we have investigated the role of electrostatic interactions in the crystallisation of PSD95-PDZ3. We have crystallised this domain within a pH range where the aspartate and glutamate residues are titratable. The results showed that below pH 4.0, the protein crystallised in prism-shaped crystals belonging to a trigonal space group. In contrast, above this pH value, the crystals' shape changes to long needles belonging to the orthorhombic or monoclinic space groups. The high resolution of the structures in this work allowed us to rationalise how the ionisation state of some residues might drive the formation of the different polymorphs. However, characterising the ionisation of these residues might help to understand how the internal redistribution and rewiring of electrostatic interactions take place underneath the dynamic allostery in the PSD95-PDZ3 domain [17,19–21].

2. Materials and Methods

2.1. Cloning, Expression and Purification of PSD95-PDZ3

The construct, including amino acid residues 302–402 (PSD95-PDZ3$^{302–402}$) of the PSD95 sequence, was subcloned into the pBAT4 vector (EMBL Core Facilities) by using *NcoI* and *HindIII* restriction sites. A methionine codon present in the *NcoI* site was used as a translation initiator, and a glycine residue was introduced after the first methionine to accommodate the *NcoI* restriction site in the DNA linker.

The PSD95-PDZ3 domain was overexpressed in the *E. coli* BL21 (DE3) strain [22]. In addition, cells were grown in LB media at 37 °C, and induction was achieved by adding IPTG at a final concentration of 0.2 mM when the OD_{600} reached a value of 0.6. After centrifugation, the precipitated cells were suspended in 50 mM Tris pH 7.5 and lysed in a French press. Subsequently, the cell lysate was acidified to pH 3.0 and clarified by centrifugation. The PSD95-PDZ3 domain was recovered from the supernatant by precipitation with solid ammonium sulfate, which reached 75% saturation at 4 °C. The

protein was solubilized in 400 mM NaCl and 50 mM Tris buffer (pH 7.5) and purified on a HiLoad 26/600 Superdex 75 column (Cytiva, Whashington, DC, USA), equilibrated with the same buffer. Furthermore, prior to being used for the crystallisation experiments, the protein was dialyzed and concentrated up to 30 mg/mL. The protein purity was checked by SDS-PAGE electrophoresis, and its concentration was determined spectrophotometrically using ε_{278nm} = 2985 M^{-1} cm^{-1} [23].

2.2. Crystallisation and Data Collection

The vapour-diffusion method was used with the commercial kits from Molecular Dimensions to screen the crystallisation conditions. The protein concentration for these initial screens was 30 mg/mL in a 10 mM Tris-HCl buffer, pH 8.0. An amount of 2 μL drops (1 μL protein and 1 μL reservoir solution) were equilibrated against 100 μL of reservoir solution using the 48-well MRC sitting-drop crystallisation plates. The best PSD95-PDZ3 crystals were obtained at 25 °C using 0.2 M ammonium sulfate, 30% *w/v* PEG 4000, and 0.1 M sodium acetate at pH 4.6. The crystallisation conditions were optimised using a hanging-drop set-up in a 24-well Linbro crystallisation plate. In addition, for this purpose, 4 μL drops (2 μL protein and 2 μL reservoir solution) were equilibrated against 1000 μL of reservoir solution. The pH of the precipitant solution was assayed in the range of pH from 3.7 to 5.0. Further, the pH of the precipitant solutions was checked and adjusted, if necessary, with the help of a pH meter. In order to avoid excessive nucleation and improve the crystals' size, 5–10% glycerol was added to the protein solution. The addition of glycerol does not affect the crystal morphology. The crystals were harvested from the crystallisation drop using LithoLoops (Molecular Dimensions, Sheffield, UK) and quickly cooled in liquid nitrogen. The crystals obtained at the different pHs were reported using a Leica microscope model M205C.

The X-ray data were collected at the beamlines ID30A-3, ID30B, and ID23-2 at the ESRF (Grenoble, France) [24], and BL13-XALOC at the ALBA synchrotron (Barcelona, Spain) [25] at 100K. The data were processed using the autoPROC toolbox [26–29], and scaling was performed using Aimless from the CCP4 suite [30,31]. The statistics of data collection are compiled in Table 1.

Table 1. Data collection and refinement statistics.

	Orthorhombic-A pH 4.6	Orthorhombic-B pH 4.0	Trigonal pH 4.0	Monoclinic pH4.0
PDB entry	8AH5	8AH7	8AH4	8AH6
Wavelength (Å)	0.9677	0.7749	0.9677	0.9677
Resolution range (Å)	19.35–1.25 (1.27–1.25)	19.53–1.25 (1.27–1.25)	48.41–1.48 (1.53–1.48)	19.68–1.63 (1.66–1.63)
Space group	$P2_12_12_1$	$P2_12_12_1$	$P3_112$	$P2_1$
Unit cell (Å, °)	28.84 32.34 88.30 90 90 90	32.56 36.75 73.22 90 90 90	61.70 61.70 228.70 90 90 120	28.86 87.50 32.43 90 92.56 90
Total reflections	242,181 (3829)	99,957 (4999)	258,384 (12,939)	83,547 (4147)
Unique reflections	22,582 (754)	24,458 (1205)	53,125 (2631)	19,832 (958)
Multiplicity	10.7 (5.1)	4.1 (4.1)	4.9 (4.9)	4.2 (4.3)
Completeness (%)	95.6 (67.0)	98.4 (99.6)	98.6 (100)	98.9 (100)
Mean I/sigma(I)	9.9 (1.6)	8.2 (1.0)	12.1 (2.2)	9.6 (2.1)
Wilson B-factor ($Å^2$)	10.43	16.37	16.73	19.06
R-merge	0.125 (0.700)	0.040 (0.709)	0.067 (0.675)	0.074 (0.678)
CC1/2	0.996 (0.749)	0.999 (0.762)	0.999 (0.796)	0.998 (0.854)
R-work	0.150 (0.257)	0.160 (0.310)	0.199 (0.326)	0.167 (0.246)
R-free	0.185 (0.276)	0.198 (0.358)	0.238 (0.375)	0.181 (0.265)
CC(work)	0.97 (0.89)	0.97 (0.91)	0.96 (0.73)	0.97 (0.91)
CC(free)	0.96 (0.89)	0.96 (0.86)	0.95 (0.95)	0.97 (0.89)

Table 1. *Cont.*

	Orthorhombic-A pH 4.6	Orthorhombic-B pH 4.0	Trigonal pH 4.0	Monoclinic pH4.0
Protein residues	102	102	566	203
Solvent	171	117	516	209
RMS (bonds)	0.011	0.014	0.012	0.004
RMS (angles)	1.20	1.26	1.09	0.71
Ramachandran favored (%)	100.00	100.00	98.38	100.00
Ramachandran allowed (%)	0.00	0.00	1.62	0.00
Ramachandran outliers (%)	0.00	0.00	0.00	0.00
Average B-factor	13.85	25.51	22.94	23.01
Macromolecules	11.86	24.23	21.69	22.01
Ligands	14.91	37.27	28.21	24.38
Solvent	23.40	33.37	29.88	30.47

2.3. Structure Solution and Refinement

The structures were solved using the PHENIX suite [32]. The phasing was performed by molecular-replacement using PHASER [33] with the coordinates of the crystallographic structure of the PSD95-PDZ3 (PDB entry 3K82 [4]). In addition, model building and refinement were carried out with COOT [33] and phenix.refine (PHENIX suite) programmes [32], respectively. The final models were validated using Molprobity and PDB_REDO [34,35]. Additionally, the structure, solution, and refinement statistics are collected in Table 1. The atomic coordinates of all structures have been deposited in the Protein Data Bank (PDB) (see Table 1).

2.4. Structure Analysis

The structure analysis was performed with the Generate web server [36], and crystal contacts were analysed with the PISA server [37]. The coordinates of the crystal interfaces were downloaded from QtPISA v2.1.0 in the graphic interface of CCP4 [31]. In addition crystal structures were superimposed using the programme LSQKAB [38]. The distances between amino acids were calculated using CONTACT in the CCP4 suite [31]. The pK_a values were calculated using the program PROPKA 3.4.0, which predicts the ionisable groups' pK_a values in proteins and protein-ligand complexes based on the 3D structure. In those cases where the residues act as coupled residues, the pK_a value calculations have been performed considering the display-coupled residues option [39,40]. All figures were created with PyMOL [41].

2.5. Dynamic Light Scattering

The oligomerization state in the solution of the PDZ domain was assessed by dynamic light scattering (DLS) measurements performed at 25 °C in different buffers. The experiments were performed at a fixed angle (θ = 173°) in a Zetasizer Nano instrument (Malvern Instrument Ltd., Malvern, UK) equipped with a 10 mW helium-neon laser (λ = 632.8 nm) and a thermoelectric temperature controller. The data were analysed with Zetasizer Software 8.02 (Malvern Instrument Ltd., UK).

3. Results

3.1. Crystal Polymorphism in the PSD95-PDZ3 at Mildly Acidic pH Conditions

We have assayed the PSD95-PDZ3 crystallisation behaviour between pH 3.7 and 5.0. Under the conditions assayed, crystals grew in a few days with different morphologies depending on the pH of the precipitant solution. Figure 1 shows the pH effect on crystal growth. All the experiments were performed at least in triplicate. The crystals that grew at pH < 4.0 had a prism shape, while above pH 4.3, crystals appeared like long needles. Between pH 4.0–4.3, both crystal shapes exist in the same drop. In addition, crystals with different morphologies were separated, and data was collected from at least

three crystals of each morphology at every pH assayed. The ones with prism shapes always belonged to the trigonal space group, and those with needle shapes belonged to the orthorhombic/monoclinic space groups.
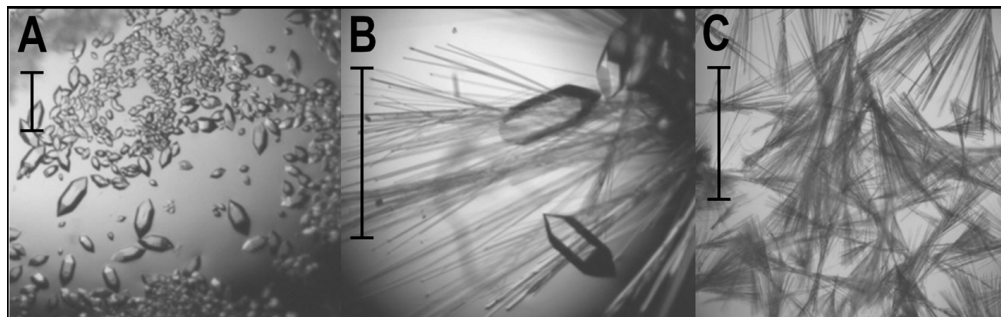

Figure 1. PSD95-PDZ3 grown in 30% PEG 4000, 0.2 M ammonium sulfate, 0.1 M sodium acetate, pH (**A**) 3.7, (**B**) 4.0, (**C**) 5.0. The crystals show different morphologies: the diamond crystals belong to the trigonal space group P3$_1$12. The long needle crystals belong to the orthorhombic space group P2$_1$2$_1$2$_1$ and monoclinic space group P2$_1$. A 200 μm bar is shown in each photograph to indicate the crystals' size.

The X-ray diffraction data demonstrated that prism-shaped crystals belong to the trigonal space group P3$_1$12. The best diffracting crystal was obtained at pH 4.0, with cell constants a = b = 61.7 Å, c = 228.7 Å, α = β = 90°, γ = 120° (PDB entry 8AH4). The asymmetric unit (AU) comprises six molecules of the PDZ domain, and this crystal structure resembles that previously reported using 0.2 M ammonium sulfate, 30% PEG 4000 as precipitant (PDB entry 6QJI [4]). The superposition of the six chains in the AU shows subtle differences, mainly located in the first and second β-turns and the carboxyl-terminal helix (α3) (Figure 2A). As in the previous trigonal structure, some residues at the amino and carboxyl terminus have not been modelled (chain A 308–401, chain B 307–401, chain C 309–401, chain D 309–400, E chain 309–402, and F chain 308–403).
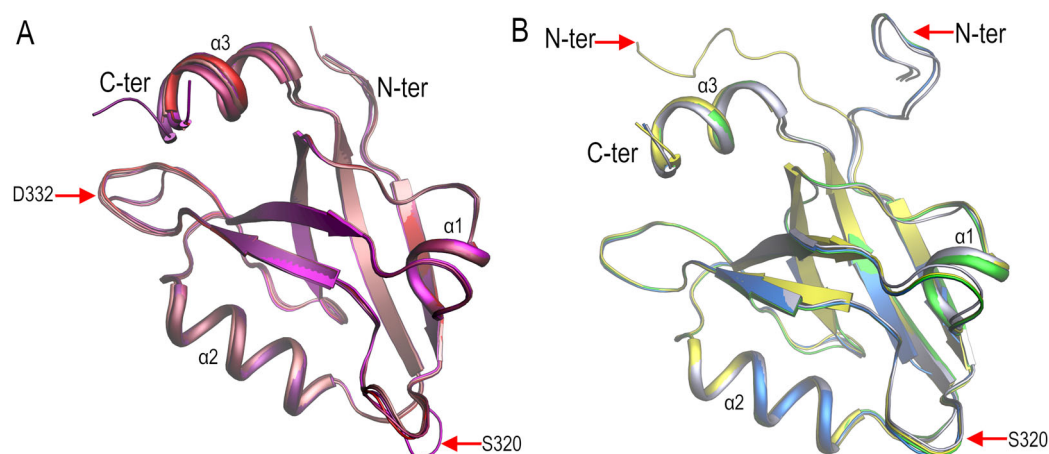

Figure 2. (**A**) Cartoon representation of the six chains in the trigonal structure (PDB entry 8AH4) coloured in red-magenta. The backbone atoms' *rmsd* value is lower than 0.5 Å, and the main differences are found in the first β-turn containing S320, next to the canonical binding site, the second β-turn (red arrows) and the extra third α-helix. (**B**) Cartoon representation of orthorhombic-A (blue, PDB entry 8HA5) and orthorhombic-B (yellow, PDB entry 8AH7) superposed to chains A (green) and B (grey) of the monoclinic structure (PDB entry 8AH6). The main differences are in the first β-turn containing S320 and the N-terminal region (red arrows), where the monoclinic structure is like orthorhombic-A, while orthorhombic-B residues 301–309 are modelled differently.

The crystals showing a needle shape belonged to two different space groups, $P2_12_12_1$ and $P2_1$. The best diffracting crystals belonging to the monoclinic space group $P2_1$ were obtained at pH 4.0 and have a unit cell a = 28.8 Å, b = 87.5 Å, c = 32.4 Å, $\alpha = \beta = 90.00°$, $\gamma = 92.56°$, containing two molecules at the AU (PDB entry 8AH6). In addition, the orthorhombic crystals show two different unit cells: a = 28.8 Å, b = 32.3 Å, c = 88.3 Å, $\alpha = \beta = \gamma = 90°$ (orthorhombic-A, PDB entry 8AH5), and a = 32.5 Å, b = 36.7 Å, c = 73.2 Å, $\alpha = \beta = \gamma = 90°$ (orthorhombic-B, PDB entry 8AH7). The best diffracting crystal of the orthorhombic-A polymorph was obtained at pH 4.6, and at pH 4.0, the crystals of the orthorhombic-B polymorph were best. Both orthorhombic crystals have a single PDZ molecule in the AU (Figure 2B).

3.2. Structural Comparison of the PDZ3-PDS95 Polymorphs Obtained at Mildly Acidic pH Conditions

We analysed the differences between the structures obtained from the needle-shape and the prims-shape crystals. The overall structure of this domain is composed of three α-helices (α1, 345–350; α2, 371–381; and α3, 394–401) and six β strands arranged in two antiparallel β-sheets (β1, 312–318; β2, 324–328; β3, 337–342; β4, 358–363; β5, 365–367; and β6, 384–391). As seen in Figure 2A, the superposition of the backbone atoms of the six chains modelled in the trigonal structure shows a low *rmsd* value (<0.5 Å). However, comparing the chains in the trigonal polymorph with those in the other polymorphs also yields a low *rmsd* value (<0.5 Å). Only those regions of the protein with high flexibility show significant differences.

As can be seen in Figure 2B, the two chains modelled in the monoclinic structure are similar to the orthorhombic-A form. However, both polymorphs have almost the same unit cell dimensions and solvent content (33%). Altogether, this suggests that the monoclinic polymorph would be a less ordered form of the orthorhombic-A crystals. On the other hand, the placement of the N-terminal region (residues 301–309) is different in the orthorhombic-B form, where two residues in this region, Asp306 and Arg309, form two saline bridges with Arg399 and Glu395, respectively. Nevertheless, this N-terminal region has not been modelled in any trigonal structure.

Other differences between the needle-shaped crystals' structures are found in the first β-turn, comprising residues Arg318-Gly322. This β-turn was modelled in a single conformation in the orthorhombic-B and monoclinic structures. Meanwhile, in the orthorhombic-A form, residues Arg318-Gly322 were modelled in two alternative conformations (Figure 3). The trigonal structure obtained at pH ≤ 4.0 shows poor electron density in this β-turn, resulting in high B-factors, which again point to the high flexibility of this region. The diverse conformations of this β-turn, next to the canonical binding site, might favour accommodating different carboxyl-terminal sequences and, in this way, facilitate the promiscuity of the PBMs' binding [42]. Further, those PDZ domains where the binding of internal sequences has been described show a flexible carboxylate-binding loop [43].
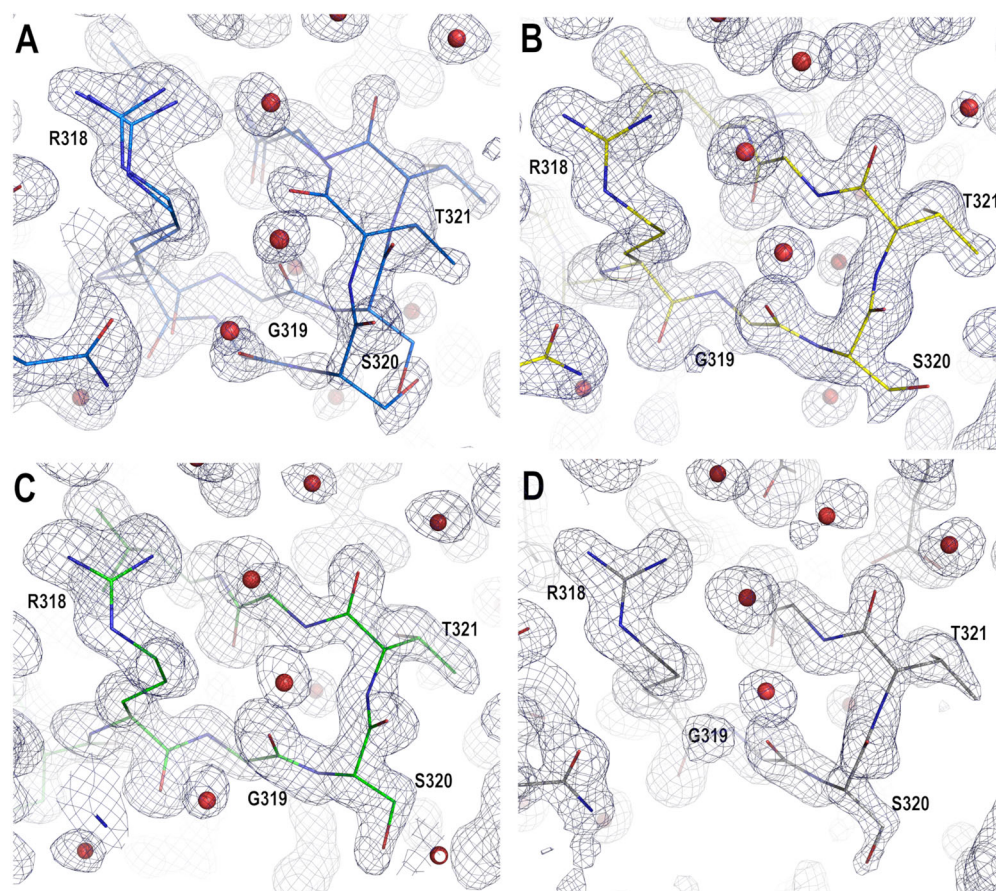
Figure 3. Difference electron density map | 2Fo-Fc | countered to 1 σ of the β-turn comprising residues Arg318-Gly322, represented as sticks, of the (**A**) orthorhombic-A (blue), (**B**) orthorhombic-B (yellow) and monoclinic chains (**C**) A (green) and (**D**) B (grey). In the orthorhombic-A, residues Arg318-Gly322 have been modelled in double conformation.

3.3. Analysis of the Electrostatic Interactions in the PSD95-PDZ3 Domain: Dependency on the pH

Previously, we reported two trigonal crystals of the PSD95-PDZ3 (PDB entries 6QJJ and 6QJI), where Asp332 plays a central role in the interactions of the primary crystal interface [4]. The sidechain of this residue interacts with residues of the canonical binding motif, imitating the interactions of the carboxyl-terminal sequences. In this work, the same interaction appears in the different polymorphs obtained between pH 3.7–5.0. As the change of space group of the crystals occurs in a short range of pH values, where the ionisation of the aspartate and glutamate residues occurs, this result would point to some role of the ionisation state of these residues in forming the different polymorphs.

In order to determine the relevance of the ionisation state of aspartate and glutamate residues in these structures, we have calculated the pK_a values using PROPKA (Table S1). We have considered that each ion-ion pair interaction has a different dielectric constant depending on the position in the protein of the two residues, their solvent exposure, and the ability of the surrounding environment to respond to changes in the electric field. Thus, these calculations have been performed in three different ways: (*a*) with the PDB coordinates file without any processing; (*b*) in those cases where more than one chain is present in the crystal structure, with the isolated chains; and (*c*) taking into account the residue's participation in the crystal contacts, generating the interface molecules. The analysis of the isolated chains mainly provides information about the changes in ionisation owed to conformational changes in the chain. Meanwhile, changes in the pK_a value calculated by procedures in *a* and *c* reveal ionisable residues' participation in the interface/crystal contacts.

The pK_a value analysis of all the isolated chains of the PSD95-PDZ3 polymorphs shows that Asp332 has a pK_a ~ 4.0. In addition to Asp332, the second β-turn also contains two glutamate residues, Glu331 and Glu334, whose pK_a values might be affected by the ionisation of their neighbouring residues. While the Asp332 pK_a value calculated in the different structures did not change, Glu331 and Glu334 pK_a values depend on the conformation of the β-turn and interactions with neighbouring residues in α2 and α3. This way, PROPKA calculations in the isolated chains show that the ionisation of Glu331 is affected by electrostatic interactions with Asp332 and His372. Meanwhile, the ionisation of the Glu334 is affected by the actual charge of Glu331, Asp332, His372, Glu396 and Glu401. Moreover, a comparison of the different structures of PSD95-PDZ3 shows different conformations for the extra domain α3 helix [4,18]. These changes are manifested in the pK_a values of the residues Glu395, Glu396, and Glu401.

Additionally, the four polymorphs show the most noticeable difference in pK_a value in the residue Asp357. In the orthorhombic and monoclinic structures, the average pK_a value is 4.1 ± 0.2; meanwhile, in the trigonal structure, the average pK_a value of the six chains is 5.4 ± 0.2. This change is also relevant because Asp357 is partially buried (~60%), and its ionisation would favour the formation of salt bridges with neighbouring arginine residues. In addition, Asp357 and Arg312 form a salt bridge in the orthorhombic and monoclinic polymorphs. However, although the Asp357 sidechain shows the same rotamer in the trigonal polymorph, the Arg312 sidechain shows a different rotamer and forms a salt bridge with Glu352 (Figure 4). The formation of this interaction results in the displacement of α1, which is transmitted to the canonical binding site.
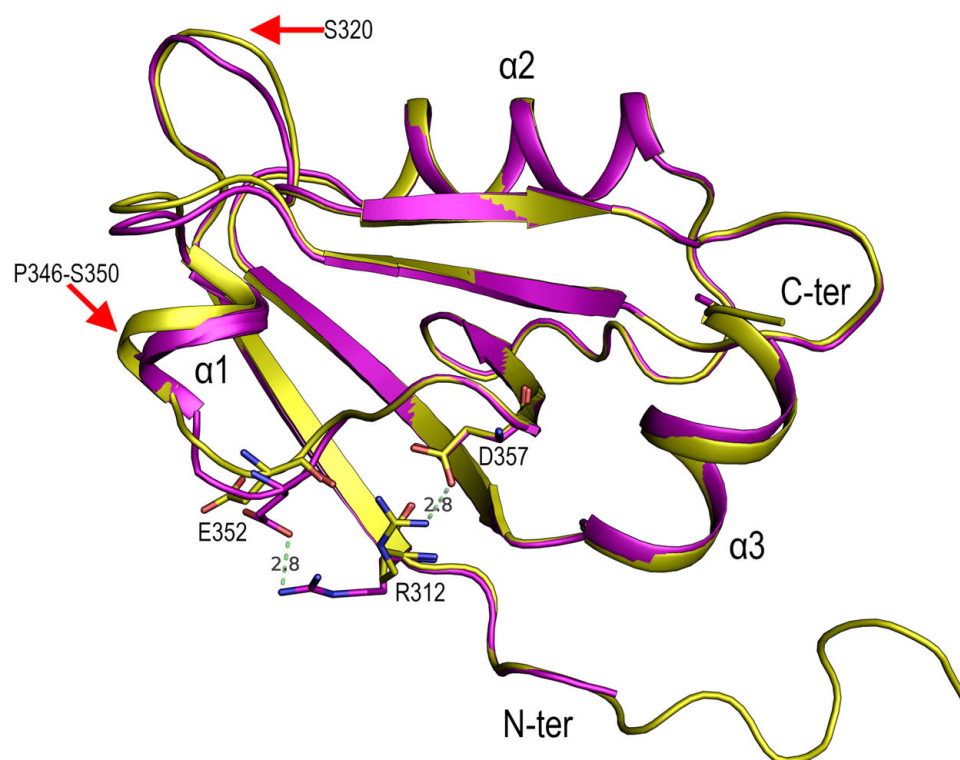

Figure 4. Comparison of the Asp357 electrostatic interactions in the orthorhombic-B (yellow) and the trigonal structures (magenta). The sidechains of the interacting residues are represented by sticks. For clarity, only chain A of the trigonal polymorph has been represented. Distances between Arg312 and Asp357 or Glu352 are marked in dashed lines (green). Red arrows indicate the most prominent differences between the orthorhombic and trigonal polymorphs: α1, residues 346–350, and the β-turn next to the canonical binding site GLGF, comprising residues 322–325.

In order to further explain the differences in the pK_a value observed in the residue Asp357, we have inspected the electron difference maps (Figure 5). In all the chains in

the trigonal form, these maps show electron density to model an acetate ion/acetic acid molecule present in the crystallisation medium. The analysis of the pK_a values of Asp357 obtained, considering the presence of this acetate molecule, increases the average value (pK_a = 7.7 $\pm$ 0.7). The acetic acid has a pK_a value of 4.76 in water but is expected to be slightly lower as the ionic strength increases. Indeed, PROPKA calculations yield a pK_a ~3.5 for ionising the acetate bound to Asp357. At pH $\leq$ 4.0, the acetate ion/acetic acid interact with the protonated Asp357, forming a favourable hydrogen bond interaction. On the contrary, the interaction would be energetically unfavourable if both the acetate and aspartate were negatively charged.
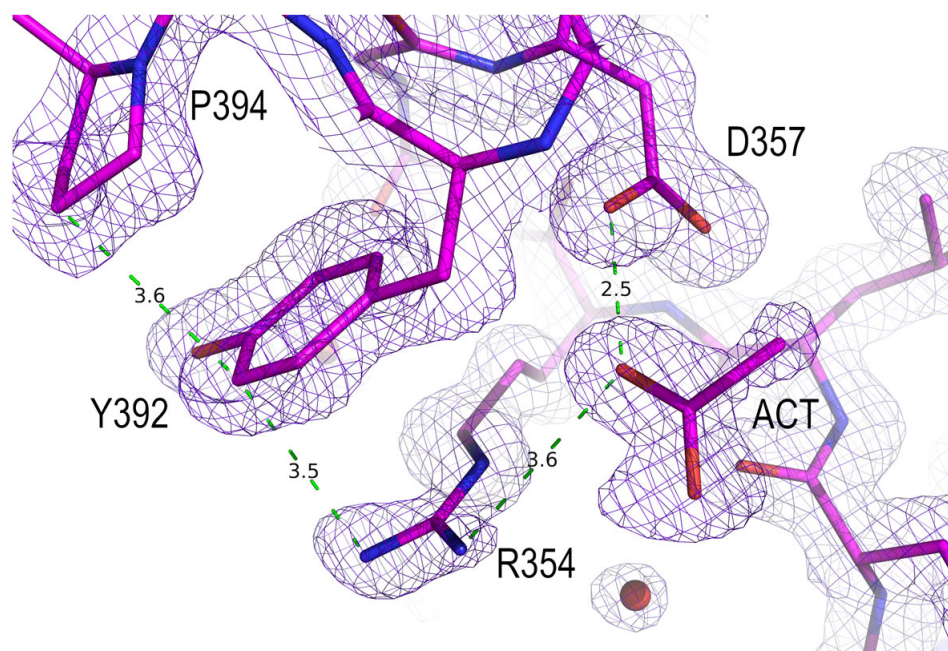

Figure 5. Interaction of the acetate ion and Asp357 in the trigonal polymorph. Difference electron density map 2Fo-Fc is countered to 1 σ.

The analysis of the electrostatic interactions provided by PROPKA also indicates the interaction between Asp357 and Arg354. The Asp357 sidechain forms a hydrogen bond with the Arg354 backbone atoms and a Coulombic interaction with its sidechain. At the same time, the Arg354 sidechain interacts with the Tyr392 through a π-stacking interaction. In this way, we can postulate that Asp357 would act as a switch to connect the canonical binding site with α3 through the alternate interaction with Arg312 or Arg354. Further, the Arg354 sidechain shows different orientations in the four polymorphs, which would point to a possible role for this residue in the communication between the extra elements of the PDZ and the canonical binding site (Figure 6).
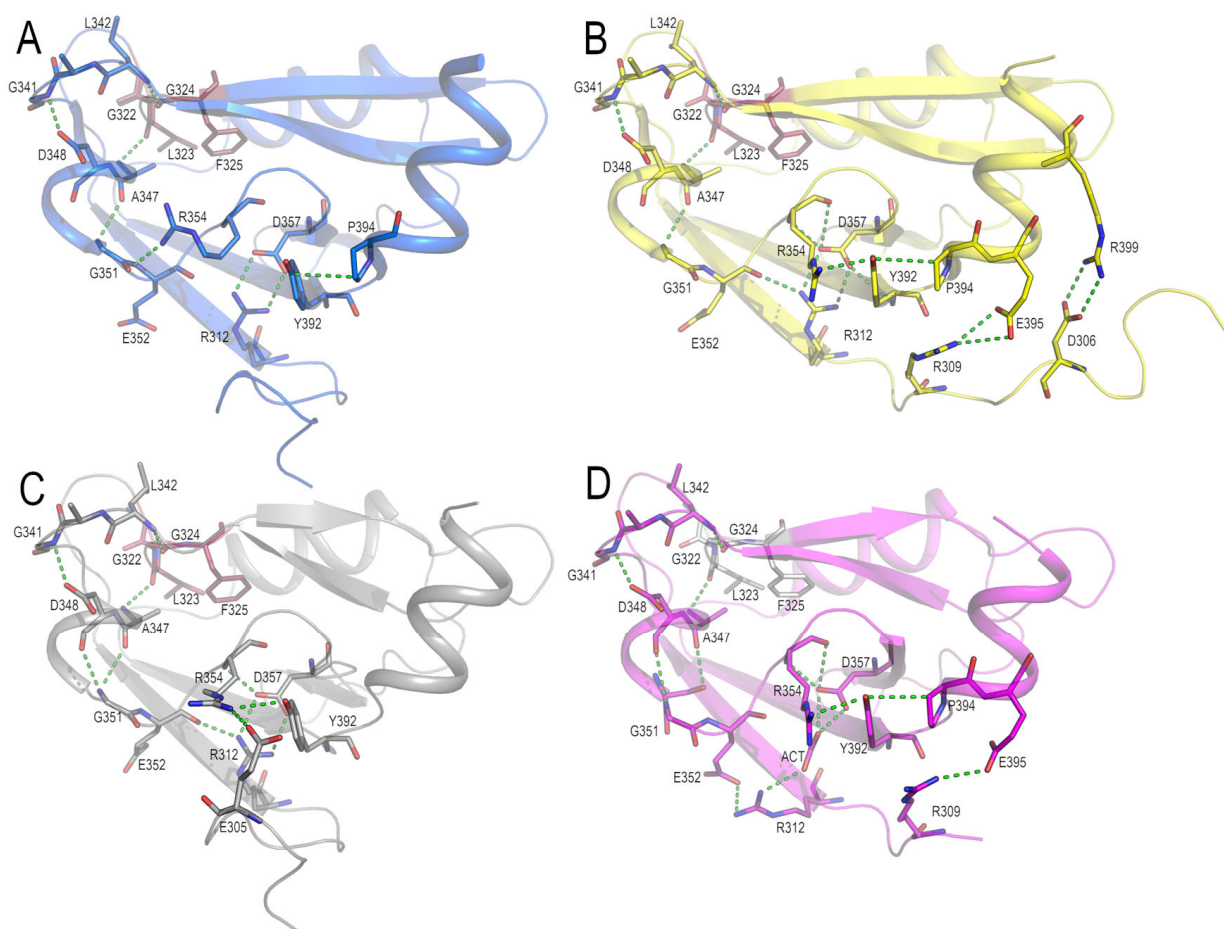
Figure 6. Electrostatic interactions in the (**A**) orthorhomic-A, (**B**) orthorhombic-B, (**C**) monoclinic and, (**D**) trigonal polymorphs. For clarity, only one chain of the monoclinic and trigonal polymorphs is shown. Residues at hydrogen bond distance are shown as sticks, and the distances have been represented with green dashed lines. Residues belonging to the canonical binding site, GLGF, have been coloured differently.

3.4. Polymorphism and Crystal Interfaces in the PSD95-PDZ3

Currently, all the crystal structures of the PSD95-PDZ3 where the residue aspartate is present in position 332 share the same main interface. The overall arrangement of the two chains in this interface is practically identical (Figure 7). However, the superposition of the backbone residues of this interface in the different crystal structures described in this work results in a very low *rmsd* value (<0.5 Å). This result suggests a specific interaction between the Asp322 sidechain and the canonical binding site. In order to check if this interaction is also present in the solution, we have performed DLS measurements between pH 3.7–5.0 using 50 mM sodium acetate buffer and at a protein concentration of 10 mg·mL^{-1}. The protein was monodispersed and displayed a hydrodynamic radius of R_{h} = 1.8 ± 0.2 nm. This R_{h} is the expected value for a monomeric PDZ domain and is equal to that obtained for the measurements performed at pH 7.0 [4]. Thus, the absence of dimeric species in the solution suggests that the crystallisation conditions promote the formation of this ubiquitous interface.
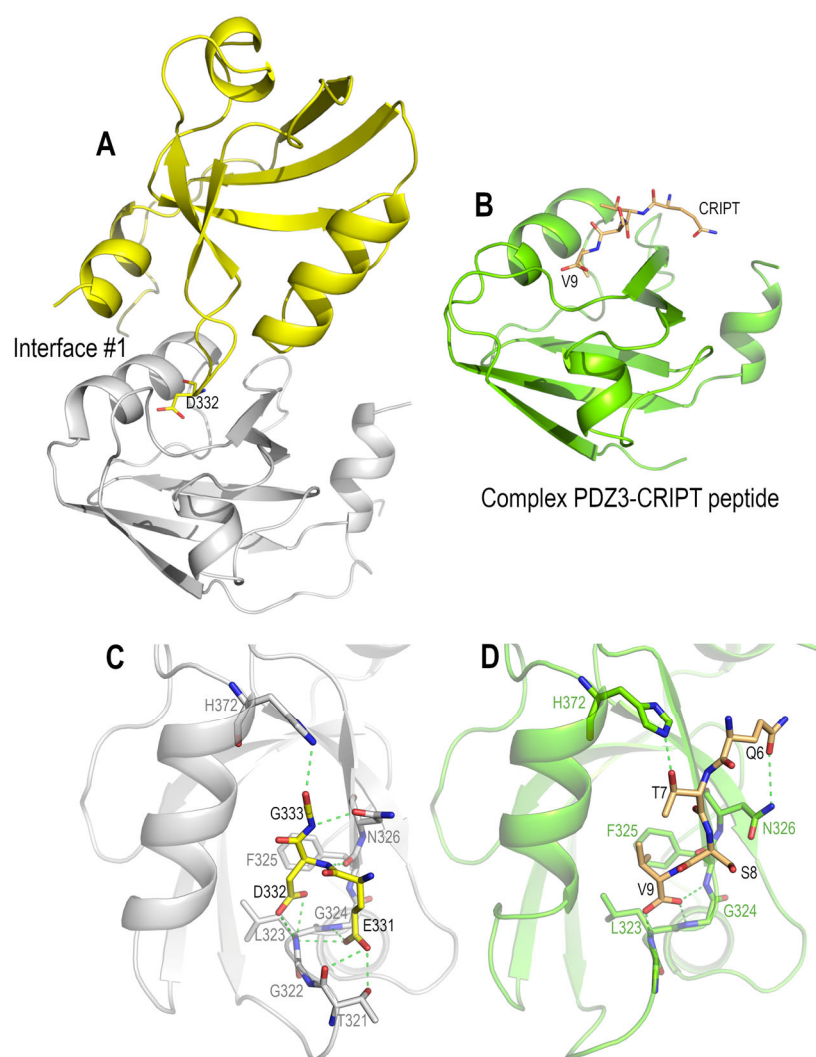
Figure 7. Comparison of the first crystal interface and the complex between PSD95-PDZ3 and CRIPT peptide (KQTSV) (PDB entry 1BE9). For the sake of clarity, only the interface in the orthorhombic-A structure is shown: (**A**) the main crystal interface (interface #1) of the orthorhombic-B (molecule 1, yellow; molecule 2, white). Asp332 is shown in sticks. (**B**) The complex structure of the PSD95-PDZ3 (cartoon, green) and CRIPT peptide (sticks, orange). The C-terminal residue, V9, is shown. (**C**) Contacts between residues Glu331-Asp332-Gly333 (sticks, yellow) and the canonical binding site of the symmetry-related molecule in the crystal interface. (**D**) Contacts between residues in the CRIPT peptide and the canonical binding site. Hydrogen bonds are shown in green dashed lines.

The four polymorphs share the main crystallographic interface, and the differences in the crystal habit must be found in the arrangement of the secondary interfaces. In using the generate web server [36], we have performed a detailed analysis of the different interfaces. Some interactions are present in all polymorphs, but the most notable difference is the packing of α2 and α3. In the monoclinic polymorph, α3 in chain A (α3A) is in contact with α2 in chain B (α2B), forming a helix-helix interaction where the helices are arranged parallelly at ~20°. The same interaction is present in the orthorhombic-A polymorph between symmetry-related molecules but not in the orthorhombic-B. In the six molecules in the AU of the trigonal structure, this interaction is only present between α2A and α3C. In this way, the polymorphs obtained below and above pH 4.0 show notable differences in the helix-helix interaction in the crystal contacts. Both helices have residues whose ionisation state might be affected by the pH of the precipitant solution (His372-Glu373-Lys380 in α2; and Glu395-Glu396-Arg399-Glu401-Lys403 in α3). The energetics of the interactions might be enhanced at those pH values where salt bridges might be established.

Other interactions that might play a role in the overall packing of the molecules in the unit cell are those arising from the different modelling of the residues 301–309 in the amino-terminal region. In this region, there are several ionisable residues that, upon changes in the pH of the solution, facilitate the interchain contacts favouring different crystal forms.

4. Discussion

4.1. Polymorphism in the PSD95-PDZ3

The crystal morphology is often pH-dependent, and changes in this parameter might favour the crystallisation of the protein in different space groups [44]. The straightforward reason for this outcome is that the pH of the precipitant solution affects the protein's protonation state and, consequently, its electrostatic field. In this way, along with ionic strength, pH is one of the most important variables influencing the solubility of proteins [45]. In order to explore the pH effect on the crystallisation of the PSD95-PDZ3, we have performed experiments in the range of pH conditions 3.7–5.0. Aspartate and glutamate have a theoretical pK_a value in the selected pH range, and these residues' ionisation might affect the crystallisation. However, it has been suggested that crystal quality might be improved at pH values near the pI of the protein [46], and the experiment's pH range was also selected because it is close to the isoelectric point of this PDZ domain (calculated pI = 5.1) [47].

Due to the fact that the surface fraction of the protein that participates in the crystal's contacts is always small, the study of polymorphs offers an opportunity to discern the protein-protein interactions responsible for crystallization. The polymorphic behaviour of the protein crystals has been broadly studied in some model proteins, for example, aprotinin (BPTI), whose polymorphic behaviour depends on pH, salt, and temperature [48–50]. Thus, BPTI has been extensively studied as a model in protein crystallisation to determine the processes that drive crystal formation [51]. As PSD95-PDZ3, BPTI is characterised by crystallising in different polymorphs at basic pH values in the presence of 1.5 M potassium phosphate at pH values next to its isoelectric point. At pH < 9.3, BPTI crystals belong to the space group P$2_1 2_1 2_1$, and a phosphate ion has been found next to Lys41. Meanwhile, at pH > 9.3, crystals belong to the space group P$2_1 2_1 2$, and the same unprotonated Lys 41 sidechain from two symmetry-related molecules is hydrogen bonded to one another [52]. The critical role of some anions bound to the protein has also been observed with the crystals obtained at acidic pHs: in the presence of thiocyanate, chloride, and sulphate ions, BPTI yield three different polymorphs in P2_1, P$6_4$22, and P$6_3$22 space groups, respectively [48]. This way, besides the pH value, some molecules in the solution might also affect the morphology of the crystals.

The analysis of the four polymorphs of the PDS95-PDZ3 under mildly acidic pH conditions shows that all the polymorphs share the same main interface in the crystal. In this interface, Asp332 plays a key role in imitating the binding of the carboxylate terminal sequences to the canonical binding site of the PDZ. The ubiquitous presence of this interface points to a preformed oligomer in the solution, as happens with the BPTI crystals obtained in acidic conditions [48]. However, at the assayed pH values, the PDS95-PDZ3 is a monomer, even with the high protein concentrations used in the crystallisation. The BPTI oligomer is preferred in the solution at high ionic strength. Thus, we cannot rule out the formation of the PDZ dimer under the crystallisation conditions.

Although the two molecules in the first interface are common to all the crystals obtained in this work, their packing in the context of the whole unit cell is diverse, giving rise to the different polymorphs. The analysis of the interactions in the crystal interfaces of the four polymorphs using PISA and the generated web servers shows that most protein-protein contacts are non-bonded. Still, some interactions are electrostatic, and the pH of the precipitant solution might be crucial to favouring one or another polymorph. The observed pK_a values of the isolated PDZ domain chains do not change much in the different polymorphs, except for the Asp357. Notably, the differences arise from the binding of a solvent acetate/acetic acid molecule to Asp357, resulting in a different arrangement of the electrostatic interactions. Indeed, these interactions might connect the extra element α3

and the canonical binding site, where some saline bridges can act as switches (Figure 7). Moreover, in the orthorhombic-B form, a saline interaction between the extra-domain N-terminal residues (301–309) and α3 residues suggests that these extra-domain residues might modulate the arrangement of the different domains in the whole PSD95 protein. However, the structure of the PSD95 is unavailable, and in the AlphaFold Protein Structure Database, the model deposited from Alphafold2 calculations (Uniprot code P78352) only accurately predicts the structure of the domains [53]. In contrast, the linker regions show low (pLDDT < 70) or very low confidence (pLDDT < 50) [54].

4.2. Role of Asp332 in the Crystallisation of the PSD95-PDZ3

The PDZ domains are among the most abundant modular domains in the human proteome and bind to specific C-terminal sequences of partner proteins [55]. The primary determinant for C-terminal peptide recognition is the conserved carboxylate-binding loop placed within the β1-β2 connecting loop and composed of residues Gly322-Leu323-Gly324-Phe325. The C-terminal carboxyl group is anchored to these residues through hydrogen bonds to the main-chain amides and the Arg318 sidechain [7]. The Asp332 sidechain imitates the role of the carboxyl-terminal residue in the crystal contacts by forming hydrogen bonds with the backbone atoms of Leu323-Gly324-Phe325 and a salt bridge with Arg318. These interactions are comparable to those found in the PSD93-PDZ3 with the CRIPT peptide (KQTSV) complex [7], where the carboxyl-terminal valine interacts through its carboxylate in the same way as the Asp332 sidechain in the crystal contact (Figure 7). Therefore, the interaction of Asp332 with the canonical binding site can be considered a pseudo-binding event since it imitates the binding of the carboxyl-terminal moiety [4]. Similarly, previous structures of the trigonal form were obtained in the presence of the peptide KKETAV (K_d = 1.5 μM [14]). However, instead of the complex, we obtained the unbound PDZ domain, where Asp332 occupied the carboxylate-binding site in the crystal contact.

The detailed analysis and comparison of the Asp332 crystal contact with the PDZ3/CRIPT complex (PDB entry 1BE9) show that, although both are alike, there are also some perceptible differences [7,21]. The structure of the complex was obtained at pH 7.2 from a protein consisting of amino acids 302–402 from PSD95 with 5 additional vector-derived residues on the N-terminus (GSPEF) and 13 on the C-terminus (NSRVNSSGRIVTN). The additional residues at the C-terminus form a β-hairpin in contact with the third alpha helix, and residues at the N-terminus. The superposition of the free form coordinates with those of the structures obtained using the sequence 302–402 shows noticeable differences in the configuration of the second β-turn. Furthermore, significant differences were found at the third alpha helix. Altogether, these structures suggest a role for the extra-domain elements in the folding and binding of carboxyl-terminal sequences to this PDZ domain [4,18]. These findings agree with the proposed role of the amino- and carboxyl-terminal regions in the allosteric modulation of this PDZ domain and its function in cell signalling [17]. The PDZ3 domain is placed between the PDZ2 and SH3 domains in the context of the PSD95 protein. In this way, the effect of the interactions established by the terminal regions might lead to a global response regarding the spatial arrangement of the protein domains upon binding with the effector ligands/proteins.

It is worth mentioning that the first crystal interface described in this work is present in all the crystal structures determined to date for the PSD95-PDZ3$^{302–402}$, except those where the Asp332 is not present. This residue has been modelled as a succinimide in two structures obtained at pH 7.5 (PDB entry 3K82) and pH 4.6 (PDB entry 3I4W). The sequence of the second β-turn makes Asp332 very susceptible to suffering this transformation [18]. This interface is also not present in the structures of the mutants Asp332Gly and Asp332Pro. In all these structures, the α3 helix was fully modelled, but Asp332 changed the electrostatics of the second β-turn. Consequently, these structures have been obtained in different polymorphs with two different conformations for this β-turn. The conformation acquired results in differences in charge distribution and the burial of some hydrophobic residues in α3, which are associated with the rearrangement of local hydrogen bonds that also affect

α2. However, these interactions would modify the helix dipole in α2 and modulate the role played by Arg318 in binding carboxyl-terminal sequences by forming a stabilising salt bridge with the terminal carboxylate [4]. Thus, modifying the electrostatic environment of α3 might significantly affect the binding of carboxyl-terminal sequences. Molecular dynamics calculations also pointed to the critical role of electrostatic interactions in a network connecting the ligand-binding site and the distant α3, as seen in the polymorphs in this work [13,17]. Furthermore, this helix has also been proposed to play a crucial role in mediating allostery in the PSD95-PDZ3 [17,20,56].

5. Conclusions

The study of polymorphism in proteins provides information about the preferred protein-protein interactions. In the protein structures that recognise specific sequences, the crystallisation process might select these interchain interactions where available. In addition, these specific interactions are found in the four polymorphs of PSD95-PDZ3 obtained in this work. These polymorphs share the main crystal interface, where the Asp332 imitates the binding of the carboxylate moiety to the canonical binding site. Similarly, as in the BPTI, not only the pH plays a role, but also the presence of some solvent molecules bound to the PDZ domain. The acetic acid/acetate ion bound to Asp357 modulates the electrostatic interactions around the extra-domain elements and facilitates the trigonal form's crystallisation at pH values ≤ 4.0. PDZ domains are characterised by promiscuity in the binding of carboxyl-terminal sequences, where the balance between polar and non-polar interactions upon binding favours this behaviour. The polymorphic structures of PSD95-PDZ3 obtained in this work provide experimental information for understanding how the electrostatic environment of key residues might modulate the binding of this PDZ domain.

References

1. Kieffer, C.; Jourdan, J.P.; Jouanne, M.; Voisin-Chiret, A.S. Noncellular screening for the discovery of protein-protein interaction modulators. *Drug Discov. Today* **2020**, *25*, 1592–1603. [CrossRef]
2. Camara-Artigas, A.; Andujar-Sanchez, M.; Ortiz-Salmeron, E.; Cuadri, C.; Casares, S. The effect of a proline residue on the rate of growth and the space group of alpha-spectrin SH3-domain crystals. *Acta Crystallogr. D Biol. Crystallogr.* **2009**, *65*, 1247–1252. [CrossRef] [PubMed]
3. Camara-Artigas, A.; Gavira, J.A.; Casares, S.; Garcia-Ruiz, J.M.; Conejero-Lara, F.; Allen, J.P.; Martinez, J.C. Understanding the polymorphic behaviour of a mutant of the alpha-spectrin SH3 domain by means of two 1.1 A resolution structures. *Acta Crystallogr. D Biol. Crystallogr.* **2011**, *67*, 189–196. [CrossRef] [PubMed]
4. Camara-Artigas, A.; Murciano-Calles, J.; Martinez, J.C. Conformational changes in the third PDZ domain of the neuronal postsynaptic density protein 95. *Acta Crystallogr. D Struct. Biol.* **2019**, *75*, 381–391. [CrossRef]

5. Elkins, J.M.; Papagrigoriou, E.; Berridge, G.; Yang, X.; Phillips, C.; Gileadi, C.; Savitsky, P.; Doyle, D.A. Structure of PICK1 and other PDZ domains obtained with the help of self-binding C-terminal extensions. *Protein Sci.* **2007**, *16*, 683–694. [CrossRef]

6. Borg, J.P. PDZ Mediated Interactions. In *PDZ MEDIATED INTERACTIONS: Methods and Protocols*; Borg, J.P., Ed.; Methods in Molecular Biology; Humana: New York, NY, USA, 2021; Volume 2256, pp. 1–292.

7. Doyle, D.A.; Lee, A.; Lewis, J.; Kim, E.; Sheng, M.; MacKinnon, R. Crystal structures of a complexed and peptide-free membrane protein-binding domain: Molecular basis of peptide recognition by PDZ. *Cell* **1996**, *85*, 1067–1076. [CrossRef] [PubMed]

8. Lee, H.J.; Zheng, J.J. PDZ domains and their binding partners: Structure, specificity, and modification. *Cell Commun. Signal* **2010**, *8*, 8. [CrossRef] [PubMed]

9. Murciano-Calles, J.; Coello, A.; Camara-Artigas, A.; Martinez, J.C. PDZ/PDZ interaction between PSD-95 and nNOS neuronal proteins: A thermodynamic analysis of the PSD95-PDZ2/nNOS-PDZ interaction. *J. Mol. Recognit.* **2020**, *33*, e2826. [CrossRef]

10. Hillier, B.J.; Christopherson, K.S.; Prehoda, K.E.; Bredt, D.S.; Lim, W.A. Unexpected modes of PDZ domain scaffolding revealed by structure of nNOS-syntrophin complex. *Science* **1999**, *284*, 812–815. [CrossRef]

11. Penkert, R.R.; DiVittorio, H.M.; Prehoda, K.E. Internal recognition through PDZ domain plasticity in the Par-6-Pals1 complex. *Nat. Struct. Mol. Biol.* **2004**, *11*, 1122–1127. [CrossRef]

12. Zhang, J.; Lewis, S.M.; Kuhlman, B.; Lee, A.L. Supertertiary structure of the MAGUK core from PSD-95. *Structure* **2013**, *21*, 402–413. [CrossRef] [PubMed]

13. Murciano-Calles, J.; Marin-Argany, M.; Cobos, E.S.; Villegas, S.; Martinez, J.C. The impact of extra-domain structures and post-translational modifications in the folding/misfolding behaviour of the third PDZ domain of MAGUK neuronal protein PSD-95. *PLoS ONE* **2014**, *9*, e98124. [CrossRef]

14. Murciano-Calles, J.; Corbi-Verge, C.; Candel, A.M.; Luque, I.; Martinez, J.C. Post-translational modifications modulate ligand recognition by the third PDZ domain of the MAGUK protein PSD-95. *PLoS ONE* **2014**, *9*, e90030. [CrossRef] [PubMed]

15. Gautier, C.; Visconti, L.; Jemth, P.; Gianni, S. Addressing the role of the α-helical extension in the folding of the third PDZ domain from PSD-95. *Sci. Rep.* **2017**, *7*, 12593. [CrossRef] [PubMed]

16. Murciano-Calles, J.; Cobos, E.S.; Mateo, P.L.; Camara-Artigas, A.; Martinez, J.C. A comparative analysis of the folding and misfolding pathways of the third PDZ domain of PSD95 investigated under different pH conditions. *Biophys. Chem.* **2011**, *158*, 104–110. [CrossRef] [PubMed]

17. Kumawat, A.; Chakrabarty, S. Hidden electrostatic basis of dynamic allostery in a PDZ domain. *Proc. Natl. Acad. Sci. USA* **2017**, *114*, E5825–E5834. [CrossRef] [PubMed]

18. Camara-Artigas, A.; Murciano-Calles, J.; Gavira, J.A.; Cobos, E.S.; Martinez, J.C. Novel conformational aspects of the third PDZ domain of the neuronal post-synaptic density-95 protein revealed from two 1.4A X-ray structures. *J. Struct. Biol.* **2010**, *170*, 565–569. [CrossRef]

19. Petit, C.M.; Zhang, J.; Sapienza, P.J.; Fuentes, E.J.; Lee, A.L. Hidden dynamic allostery in a PDZ domain. *Proc. Natl. Acad. Sci. USA* **2009**, *106*, 18249–18254. [CrossRef] [PubMed]

20. Zhang, J.; Petit, C.M.; King, D.S.; Lee, A.L. Phosphorylation of a PDZ domain extension modulates binding affinity and interdomain interactions in postsynaptic density-95 (PSD-95) protein, a membrane-associated guanylate kinase (MAGUK). *J. Biol. Chem.* **2011**, *286*, 41776–41785. [CrossRef]

21. Raman, A.S.; White, K.I.; Ranganathan, R. Origins of Allostery and Evolvability in Proteins: A Case Study. *Cell* **2016**, *166*, 468–480. [CrossRef]

22. Murciano-Calles, J.; Cobos, E.S.; Mateo, P.L.; Camara-Artigas, A.; Martinez, J.C. An oligomeric equilibrium intermediate as the precursory nucleus of globular and fibrillar supramacromolecular assemblies in a PDZ domain. *Biophys. J.* **2010**, *99*, 263–272. [CrossRef]

23. Gill, S.C.; von Hippel, P.H. Calculation of protein extinction coefficients from amino acid sequence data. *Anal. Biochem.* **1989**, *182*, 319–326. [CrossRef] [PubMed]

24. Bowler, M.W.; Svensson, O.; Nurizzo, D. Fully automatic macromolecular crystallography: The impact of MASSIF-1 on the optimum acquisition and quality of data. *Crystallogr. Rev.* **2016**, 1–17. [CrossRef]

25. Juanhuix, J.; Gil-Ortiz, F.; Cuni, G.; Colldelram, C.; Nicolas, J.; Lidon, J.; Boter, E.; Ruget, C.; Ferrer, S.; Benach, J. Developments in optics and performance at BL13-XALOC, the macromolecular crystallography beamline at the ALBA synchrotron. *J. Synchrotron Radiat.* **2014**, *21*, 679–689. [CrossRef] [PubMed]

26. Kabsch, W. XDS. *Acta Crystallogr. D Biol. Crystallogr.* **2010**, *66*, 125–132. [CrossRef]

27. Kabsch, W. Integration, scaling, space-group assignment and post-refinement. *Acta Crystallogr. D Biol. Crystallogr.* **2010**, *66*, 133–144. [CrossRef] [PubMed]

28. Vonrhein, C.; Flensburg, C.; Keller, P.; Sharff, A.; Smart, O.; Paciorek, W.; Womack, T.; Bricogne, G. Data processing and analysis with the autoPROC toolbox. *Acta Crystallogr. D Biol. Crystallogr.* **2011**, *67*, 293–302. [CrossRef]

29. Vonrhein, C.; Tickle, I.J.; Flensburg, C.; Keller, P.; Paciorek, W.; Sharff, A.; Bricogne, G. Advances in automated data analysis and processing within autoPROC, combined with improved characterisation, mitigation and visualisation of the anisotropy of diffraction limits using STARANISO. *Acta Crystallogr. Sect. A* **2018**, *74*, a360. [CrossRef]

30. Evans, P.R.; Murshudov, G.N. How good are my data and what is the resolution? *Acta Crystallogr. D Biol. Crystallogr.* **2013**, *69*, 1204–1214. [CrossRef]

31. Winn, M.D.; Ballard, C.C.; Cowtan, K.D.; Dodson, E.J.; Emsley, P.; Evans, P.R.; Keegan, R.M.; Krissinel, E.B.; Leslie, A.G.; McCoy, A.; et al. Overview of the CCP4 suite and current developments. *Acta Crystallogr. D Biol. Crystallogr.* **2011**, *67*, 235–242. [CrossRef]

32. Liebschner, D.; Afonine, P.V.; Baker, M.L.; Bunkoczi, G.; Chen, V.B.; Croll, T.I.; Hintze, B.; Hung, L.-W.; Jain, S.; McCoy, A.J.; et al. Macromolecular structure determination using X-rays, neutrons and electrons: Recent developments in Phenix. *Acta Crystallogr. Sect. D* **2019**, *75*, 861–877. [CrossRef] [PubMed]

33. Bunkoczi, G.; Echols, N.; McCoy, A.J.; Oeffner, R.D.; Adams, P.D.; Read, R.J. Phaser.MRage: Automated molecular replacement. *Acta Crystallogr. D Biol. Crystallogr.* **2013**, *69*, 2276–2286. [CrossRef]

34. Chen, V.B.; Arendall, W.B., 3rd; Headd, J.J.; Keedy, D.A.; Immormino, R.M.; Kapral, G.J.; Murray, L.W.; Richardson, J.S.; Richardson, D.C. MolProbity: All-atom structure validation for macromolecular crystallography. *Acta Crystallogr. D Biol. Crystallogr.* **2010**, *66*, 12–21. [CrossRef] [PubMed]

35. Joosten, R.P.; Long, F.; Murshudov, G.N.; Perrakis, A. The PDB_REDO server for macromolecular structure model optimization. *IUCrJ* **2014**, *1*, 213–220. [CrossRef] [PubMed]

36. Laskowski, R.A. PDBsum new things. *Nucleic Acids Res.* **2009**, *37*, D355–D359. [CrossRef] [PubMed]

37. Krissinel, E. Macromolecular complexes in crystals and solutions. *Acta Crystallogr. D Biol. Crystallogr.* **2011**, *67*, 376–385. [CrossRef]

38. Kabsch, W. A solution for the best rotation to relate two sets of vectors. *Acta Crystallogr. Sect. A* **1976**, *32*, 922–923. [CrossRef]

39. Søndergaard, C.R.; Olsson, M.H.M.; Rostkowski, M.; Jensen, J.H. Improved Treatment of Ligands and Coupling Effects in Empirical Calculation and Rationalization of pKa Values. *J. Chem. Theory Comput.* **2011**, *7*, 2284–2295. [CrossRef]

40. Olsson, M.H.; Sondergaard, C.R.; Rostkowski, M.; Jensen, J.H. PROPKA3: Consistent Treatment of Internal and Surface Residues in Empirical pKa Predictions. *J. Chem. Theory Comput.* **2011**, *7*, 525–537. [CrossRef]

41. *The PyMOL Molecular Graphics System*, Version 2.0; Schrodinger, LLC.: New York, NY, USA, 2015.

42. Basdevant, N.; Weinstein, H.; Ceruso, M. Thermodynamic basis for promiscuity and selectivity in protein-protein interactions: PDZ domains, a case study. *J. Am. Chem. Soc.* **2006**, *128*, 12766–12777. [CrossRef]

43. Mu, Y.; Cai, P.; Hu, S.; Ma, S.; Gao, Y. Characterization of diverse internal binding specificities of PDZ domains by yeast two-hybrid screening of a special peptide library. *PLoS ONE* **2014**, *9*, e88286. [CrossRef]

44. McPherson, A.; Cudney, B. Optimization of crystallization conditions for biological macromolecules. *Acta crystallogr. Sect. F, Struct. Biol. Commun.* **2014**, *70*, 1445–1467. [CrossRef]

45. McPherson, A.; Gavira, J.A. Introduction to protein crystallization. *Acta Crystallogr. F Struct. Biol. Commun.* **2014**, *70*, 2–20. [CrossRef] [PubMed]

46. Kantardjieff, K.A.; Rupp, B. Protein isoelectric point as a predictor for increased crystallization screening efficiency. *Bioinformatics* **2004**, *20*, 2162–2168. [CrossRef]

47. Wilkins, M.R.; Gasteiger, E.; Bairoch, A.; Sanchez, J.C.; Williams, K.L.; Appel, R.D.; Hochstrasser, D.F. Protein identification and analysis tools in the ExPASy server. *Methods Mol. Biol.* **1999**, *112*, 531–552. [CrossRef]

48. Hamiaux, C.; Perez, J.; Prange, T.; Veesler, S.; Ries-Kautt, M.; Vachette, P. The BPTI decamer observed in acidic pH crystal forms pre-exists as a stable species in solution. *J. Mol. Biol.* **2000**, *297*, 697–712. [CrossRef]

49. Hamiaux, C.; Prange, T.; Ries-Kautt, M.; Ducruix, A.; Lafont, S.; Astier, J.P.; Veesler, S. The decameric structure of bovine pancreatic trypsin inhibitor (BPTI) crystallized from thiocyanate at 2.7 A resolution. *Acta Crystallogr. D Biol. Crystallogr.* **1999**, *55*, 103–113. [CrossRef] [PubMed]

50. Grouazel, S.; Bonneté, F.; Astier, J.-P.; Ferté, N.; Perez, J.; Veesler, S. Exploring Bovine Pancreatic Trypsin Inhibitor Phase Transitions. *J. Phys. Chem. B* **2006**, *110*, 19664–19670. [CrossRef] [PubMed]

51. Lubkowski, J.; Wlodawer, A. Decamers observed in the crystals of bovine pancreatic trypsin inhibitor. *Acta Crystallogr. D Biol. Crystallogr.* **1999**, *55*, 335–337. [CrossRef]

52. Gallagher, W.H.; Croker, K.M. Identification of a molecular switch that selects between two crystals forms of bovine pancreatic trypsin inhibitor. *Protein Sci.* **1994**, *3*, 1602–1604. [CrossRef] [PubMed]

53. Varadi, M.; Anyango, S.; Deshpande, M.; Nair, S.; Natassia, C.; Yordanova, G.; Yuan, D.; Stroe, O.; Wood, G.; Laydon, A.; et al. AlphaFold Protein Structure Database: Massively expanding the structural coverage of protein-sequence space with high-accuracy models. *Nucleic Acids Res.* **2021**, *50*, D439–D444. [CrossRef]

54. Jumper, J.; Evans, R.; Pritzel, A.; Green, T.; Figurnov, M.; Ronneberger, O.; Tunyasuvunakool, K.; Bates, R.; Žídek, A.; Potapenko, A.; et al. Highly accurate protein structure prediction with AlphaFold. *Nature* **2021**, *596*, 583–589. [CrossRef] [PubMed]

55. Ernst, A.; Appleton, B.A.; Ivarsson, Y.; Zhang, Y.; Gfeller, D.; Wiesmann, C.; Sidhu, S.S. A Structural Portrait of the PDZ Domain Family. *J. Mol. Biol.* **2014**, *426*, 3509–3519. [CrossRef] [PubMed]

56. Reynolds, K.A.; McLaughlin, R.N.; Ranganathan, R. Hot spots for allosteric regulation on protein surfaces. *Cell* **2011**, *147*, 1564–1575. [CrossRef] [PubMed]